

Extracting a stimulus-unlocked component from EEG during NoGo trials of a Go/NoGo task

Yusuke Takeda, Kentaro Yamanaka, Daichi Nozaki, and Yoshiharu Yamamoto*

Educational Physiology Laboratory, Graduate School of Education, The University of Tokyo, 7-3-1 Hongo, Bunkyo-ku, Tokyo 113-0033, Japan

Received 22 October 2007; revised 5 March 2008; accepted 10 March 2008
Available online 20 March 2008

Like electroencephalographic (EEG) activity during reaction time tasks, EEG activity during tasks without overt responses may also consist of two components: stimulus-locked and -unlocked components. The extraction of such stimulus-unlocked components has been difficult owing to the unknown delays. Here, we propose a novel method to extract both of the two components from single-channel EEG epochs. In this method, we initially set random values for the delays and extract uncontaminated stimulus-locked and -unlocked components using the preset delays and a discrete Fourier transform. Then, we reconstruct the EEG by overlapping the extracted components with the preset delays, and calculate the residual errors between the reconstructed and original EEG. This procedure is repeated by updating the delays until the residual errors become adequately small. After verifying the performance of this method by two kinds of simulations with artificial and EEG data, we apply the method to EEG during NoGo trials of a Go/NoGo task, and obtain the stimulus-unlocked components, the magnitudes of which are comparable with those of the stimulus-locked components. By applying this method, it is possible to study internal and subjective brain activity, which occurs with variable delays.

© 2008 Elsevier Inc. All rights reserved.

Keywords: Stimulus-locked component; Stimulus-unlocked component; NoGo trial; Go/NoGo task; Electroencephalography (EEG)

Introduction

When a subject responds overtly to a stimulus, brain activity consists of two components: a component time-locked to the stimulus, i.e., a stimulus-locked component, and a component not time-locked to the stimulus but to the response, i.e., a response-locked component (Braun et al., 2002; Endo et al., 1999; Goodin et al., 1986; Jung et al., 2001; Lamarre et al., 1983; Nelson, 1987;

Nelson et al., 1991; Perfiliev, 1998; Tanji and Kurata, 1982). In the human scalp electroencephalography (EEG) studies, these components are conventionally extracted by averaging EEG epochs with respect to either stimulus or response onset to increase the signal to noise ratio (SNR). However, when the two components are temporally overlapping, the two components are mutually contaminated by the averaging procedure (Kok, 1988; Verleger, 1988; Verleger et al., 2006). To solve this problem, we recently proposed a method to extract the uncontaminated components from each channel of EEG epochs and reaction times (RTs) (described in the Methods section), and applied the method to the EEG during an auditory simple reaction time task (Takeda et al., 2008).

However, even when a subject does not respond overtly to a stimulus, EEG activity may exhibit two components: a stimulus-locked component, and a component not time-locked to the stimulus but to a certain event in the brain (David et al., 2006; Haenschel et al., 2000; Schürmann and Başar, 2001; Tallon-Baudry et al., 1996; Tallon-Baudry and Bertrand, 1999); here, the latter is called the stimulus-unlocked component, defined as the EEG component which has a fixed waveform and of which the delay fluctuates from trial to trial. However, such a stimulus-unlocked component cannot be extracted by the averaging procedure, or even by our previous method (Takeda et al., 2008), because its delays in individual trials are of unknown length. Although, using time-frequency analyses, some studies indicate that EEG activity during various cognitive tasks involves some stimulus-unlocked oscillatory components together with stimulus-locked components (David et al., 2006; Haenschel et al., 2000; Jung-Beeman et al., 2004; Kirmizi-Alsan et al., 2006; Tallon-Baudry et al., 1996; Tallon-Baudry and Bertrand, 1999), suggestive of the presence of the stimulus-unlocked components, their waveforms and the delays of individual trials have not been identified. Because the brain activity related to a complex function, e.g., attention, memory and problem solving, occurs in a stimulus-unlocked way, it is important to develop a method for extracting the waveform and delays of the stimulus-unlocked brain activity.

In this paper, we thus propose a novel method to estimate the delays of the stimulus-unlocked component, and to extract the

* Corresponding author. Fax: +81 3 5689 8069.

E-mail address: yamamoto@p.u-tokyo.ac.jp (Y. Yamamoto).

Available online on ScienceDirect (www.sciencedirect.com).

stimulus-locked and -unlocked components only from single-channel EEG epochs. In this method, the delays are estimated by solving an optimization problem, in which our previous method (Takeda et al., 2008) is used for decomposing EEG into the two components. We examine the performance of this method by two types of simulation tests with artificial and EEG data respectively. Then, we apply this method to EEG data during NoGo trials of a Go/NoGo task, in which subjects are instructed to withhold a response.

Methods

Extraction of stimulus-locked and -unlocked components

It is assumed that brain activity during a cognitive task consists of stimulus-locked activity, stimulus-unlocked activity shifted by a delay of unknown length, and noise. Therefore, observed single-channel EEG data can be expressed by:

$$y_n(t) = s(t) + r(t - \tau_n) + v_n(t) \quad (t = 0, \dots, T - 1; n = 1, \dots, N), \quad (1)$$

where $y_n(t)$: observed EEG data in trial n ; $s(t)$: stimulus-locked component; $r(t)$: stimulus-unlocked (or response-locked, if there is an overt response) component; τ_n : delay of $r(t)$ in trial n ; $v_n(t)$: noise in trial n . Here, the objective is to obtain $s(t)$, $r(t)$ and τ_n only from $y_n(t)$.

Once a set of delays $\tau = [\tau_1, \tau_2, \dots, \tau_N]$ is determined, the waveforms of $s(t)$ and $r(t)$ are determined by our previous method (Takeda et al., 2008). In our previous method, to extract $s(t)$ and $r(t)$ separately, Eq. (1) and the average across n of Eq. (1) are solved simultaneously for $s(t)$ and $r(t)$ in the Fourier domain, and the

solutions are averaged across n . As a result, $s(t)$ and $r(t)$ extracted by using τ are respectively expressed by:

$$s_\tau(t) = \text{IDFT} \left[\frac{1}{N} \sum_{n=1}^N \frac{\exp(-i2\pi\omega\tau_n/T) \bar{Y}(\omega) - \bar{E}(\omega) Y_n(\omega)}{D(n, \omega)} \right], \quad (2)$$

$$r_\tau(t) = \text{IDFT} \left[\frac{1}{N} \sum_{n=1}^N \frac{Y_n(\omega) - \bar{Y}(\omega)}{D(n, \omega)} \right], \quad (3)$$

where

$$D(n, \omega) = \begin{cases} c & \omega = 0 \\ \exp(-i2\pi\omega\tau_n/T) - \bar{E}(\omega) & \omega \neq 0 \end{cases}; \quad (4)$$

$Y_n(\omega)$: discrete Fourier transform of $y_n(t)$; $\bar{Y}(\omega)$: average across n of $Y_n(\omega)$; $\bar{E}(\omega)$: average across n of $\exp(-i2\pi\omega\tau_n/T)$; $\text{IDFT}[\cdot]$: inverse discrete Fourier transform of \cdot ; c in Eq. (4): a constant number, being set to unity in this study (see Takeda et al., 2008, for detailed descriptions).

We estimate true τ under a certain assumption. Fig. 1 shows the simulation results on which the assumption is based. If τ is true, the waveforms of $s_\tau(t)$ and $r_\tau(t)$ are close to those of $s(t)$ and $r(t)$ (Fig. 1, C), and the waveform of $s_\tau(t) + r_\tau(t - \tau_n)$ becomes close to $y_n(t)$ (Fig. 1, E). In contrast, if τ is wrong, the waveforms of $s_\tau(t)$ and $r_\tau(t)$ are not close to those of $s(t)$ and $r(t)$ (Fig. 1, D), and the waveform of $s_\tau(t) + r_\tau(t - \tau_n)$ does not become close to $y_n(t)$ (Fig. 1, F). Based on these simulation results, we assume that sets of nearly true delays provide better approximations of the observed EEG data than sets of wrong delays. Under

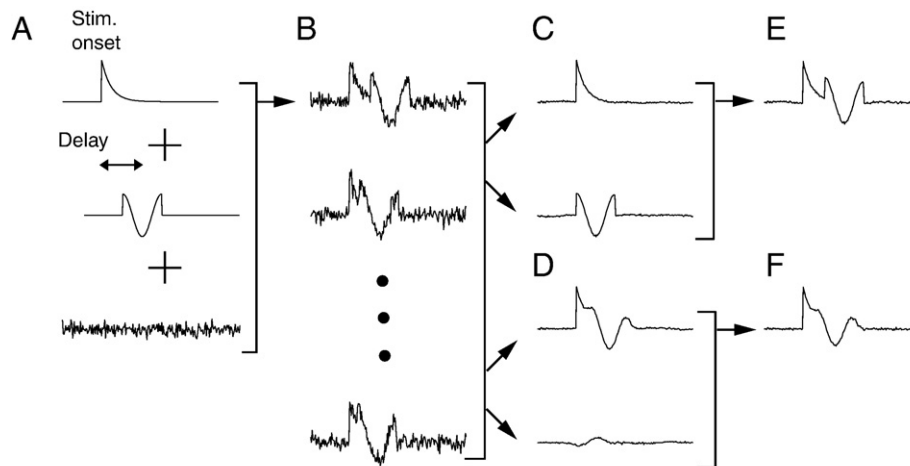


Fig. 1. Simulation results on which the proposed method is based. (A) Original stimulus-locked component (top), original stimulus-unlocked component (middle), and noise (bottom). (B) Simulated data obtained by Eq. (1). (C) Stimulus-locked component (top) and stimulus-unlocked component (bottom) extracted by our previous method using the true τ (Takeda et al., 2008). The waveforms of these components are similar to those of the original ones. (D) Stimulus-locked component (top) and stimulus-unlocked component (bottom) extracted by our previous method using the wrong τ (Takeda et al., 2008). The waveforms of these components are different from those of the original ones. (E) Reconstructed data from the components extracted by the true τ . Its waveform is similar to that of the simulated data (top row in B). (F) Reconstructed data from the components extracted by the wrong τ . Its waveform is different from that of the simulated data (top row in B).

this assumption, we estimate the true τ by solving an optimization problem of:

$$\text{Minimize } o_\tau = \sum_{t=t_1}^{t_2} \sum_{n=1}^N \{y_n(t) - s_\tau(t) - r_\tau(t - \tau_n)\}^2$$

Subject to $\tau \subset N$.

In this study, t_1 and t_2 were respectively set at 0 and 1000 ms after the stimulus onset.

To select algorithms for solving this optimization problem, by using simulated data (not shown), we checked the structure of the objective function by changing τ_k (k was fixed) one step at a time. Consequently, as the objective function seemed to have many local minima, hill-climbing methods, such as the steepest descent method, are not suitable because these methods are easily trapped in a local minimum. Stochastic algorithms, such as simulated annealing (Kirkpatrick et al., 1983), are thus considered suitable because these methods can escape from a local minimum and find a global minimum. Among the algorithms we tested, a random search (Zhihgljavsky, 1991) is the best in the points that this algorithm achieves speedy convergence to a global minimum with a high probability. The procedure of the random search is as follows:

1. Generate a set of delays τ by random numbers, and set the index of the delays k to 1.
2. Obtain o_τ .
3. Make τ' by changing τ_k in τ randomly.
4. Obtain $o_{\tau'}$.
5. Replace τ and o_τ by τ' and $o_{\tau'}$ respectively if $o_{\tau'}$ is smaller than o_τ .
6. Return to step 3 with increasing k by 1 (k returns to 1 if k becomes larger than N).

This procedure is different from the so-called general random search (Zhihgljavsky, 1991) in the point that, at step 3 in each iteration, this procedure does not change all of the $\tau_n(n=1, \dots, N)$, but only one τ_k , where k circulates from 1 to N as the iteration number increases.

By using $y_n(n=1, \dots, N)$ shown in Fig. 1, B, we demonstrate the performance of the random search in Fig. 2. Fig. 2, A, shows how the values of the objective function decrease within the same

computational time (10 s) by the following four algorithms: the random search, a more general random search (Zhihgljavsky, 1991) where the procedure was the same as one we used except for making τ' by random numbers at step 3, a genetic algorithm (Holland, 1975) and simulated annealing (Kirkpatrick et al., 1983). The convergence of the random search is the fastest among these (Fig. 2, A). Fig. 2, B, shows the converged points by 2000 [= $20 \times N(N=100)$] iterations of the random search, taking about 13 s by our personal computer [Dell XPS M1210 Intel(R) Core(TM)2 CPU T7200 at 2.00 GHz]. The 2000 iterations were repeated 100 times with different initial τ at step 1. Among the 100 converged points, 54 points (encircled points in Fig. 2, B) reached values smaller than 200, and the correlation coefficients between the estimated and original delays were higher than 0.94. This indicates that the random search achieves convergence to a global minimum with a probability of about 0.5, being adequately high for practical use.

In the optimization, we firstly repeated $20 \times N$ iterations of the random search for 50 times, and obtained 50 sets of τ and o_τ . Then, we started $20 \times N$ iterations from the τ which had the smallest o_τ among the 50 sets.

During the optimization, we monitored the variance across n of $y_n(t) - s_\tau(t) - r_\tau(t - \tau_n)$, which became smaller and smaller as the optimization proceeded, and stopped the optimization if the variance became smaller than those of the pre-stimulus level. This is because $y_n(t) - s_\tau(t) - r_\tau(t - \tau_n)$ is considered as the extracted background noise and the level of original background noise is considered not to decrease after stimulus onsets.

After the optimization, we adjusted the average of the obtained τ . This adjustment is required because the average of τ varies depending on the time point defined as the onset of the stimulus-unlocked component and the onset is arbitrarily determined in the optimization. For example, we adjusted the average of τ obtained from the EEG during NoGo trials so that the maximum peaks in the extracted stimulus-unlocked components became their onsets (described in the Data analysis subsection). We then called the adjusted τ the estimated delays.

Simulation tests

To examine the performance of the proposed method for artificial and EEG-like data, we conducted two simulation tests: a simulation with artificial data and a simulation with EEG data.

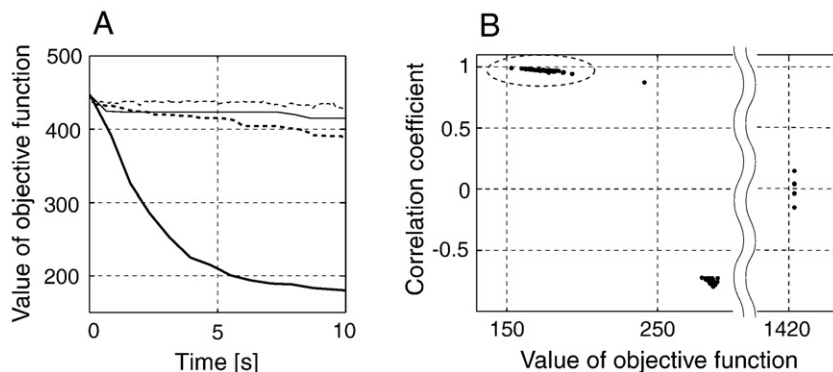


Fig. 2. Performance of a random search. (A) Decay of the values of the objective function by the restricted random search proposed (thick solid line), completely random search (thin solid line), genetic algorithm (thick dotted line), and simulated annealing (thin dotted line). (B) Scatter plots of the converged values of the objective function and the correlation coefficients between the estimated and original delays by the restricted random search. Encircled dots indicate the converged points whose values of the objective function are lower than 200.

In the simulation with artificial data, original $s(t)$ and $r(t)$ were generated by the exponential and the cosine functions respectively (Fig. 1, A). Gaussian random numbers [mean=270 ms, standard deviation (SD)=50 ms] were used as τ , and white noise was used as $v_n(t)$. To examine the relation between the accuracy of the estimated τ and noise level, we generated 11 sets of $y_n(t)(n=1, \dots, 100)$ with different SNRs of $-10, -9, \dots, 0$ by adjusting SD of $v_n(t)$ to 0.56, 0.50, 0.45, 0.39, 0.36, 0.32, 0.28, 0.25, 0.22, 0.20, 0.18, respectively. The SNR was defined as $10 \log_{10} \left(\frac{\sum_{t=0}^{T-1} r(t)^2}{\sum_{t=0}^{T-1} v_n(t)^2} \right)$.

In the simulation with EEG data, the stimulus- and response-locked components extracted by our previous method (Takeda et al., 2008) from all the subjects' EEG and RTs during Go trials in the Go/NoGo task (described in Experimental procedure and Data analysis subsections) were used as $s(t)$ and $r(t)$ respectively, and the RTs, which were randomly selected from all the subjects' RTs during Go trials, were used as τ . Noise $v_n(t)(n=1, \dots, 100)$ was obtained from all the subjects' EEG during a passive viewing task (described in Experimental procedure and Data analysis subsections) in the following way. The averaged EEG across trials was subtracted from each of the sets of EEG data, and the resultant EEG was discrete Fourier transformed and new sweeps were constructed by randomizing the phase information of the transformed EEG, while keeping their distributions constant. From the sweeps obtained, we randomly selected 100 sweeps, and used them as $v_n(t)(n=1, \dots, 100)$. To examine the relation between the accuracy of the estimated τ and the noise level, we generated 11 sets of $y_n(t)(n=1, \dots, 100)$ with different SNRs of $-10, -9, \dots, 0$ by adjusting SD of $v_n(t)$ to 2.6, 2.3, 2.0, 1.8, 1.6, 1.4, 1.3, 1.2, 1.0,

0.91, 0.81, respectively. Without the adjustment, SD of $v_n(t)$ was 6.8 and the SNR was -18 .

Because our method uses a stochastic algorithm (the random search) in the optimization, the estimation results should vary more or less in every estimation. To examine the robustness of the estimation results, we applied the proposed method to each set of $y_n(t)(n=1, \dots, 100)$ for 10 times, and obtained 10 sets of τ , $s_\tau(t)$ and $r_\tau(t)$ for each set. Because the averages of τ were arbitrarily determined in the optimization, we adjusted the averages of τ to those of the original τ . The accuracy of the estimated τ was quantified by the correlation coefficient between the estimated and original τ (Figs. 3 and 4, D). Also, the similarity of the extracted component to the original one was quantified by the correlation coefficient between them, corresponding to the cross correlation between them at the lag of zero.

Experimental procedure

Nine healthy adults (aged 28.4 ± 3.7 years) constituted the experimental population. All the subjects gave their informed consent and the local ethics committee approved the experimental procedure.

The subjects were comfortably seated on a chair in a dimly lit, electrically shielded room. At about 50 cm in front of the subjects' eyes, red and green light-emitting diodes (LEDs) for imperative signals were vertically arrayed 1.5 cm apart on a black panel. The subjects were instructed to perform two kinds of tasks in the following order: a Go/NoGo task and a passive

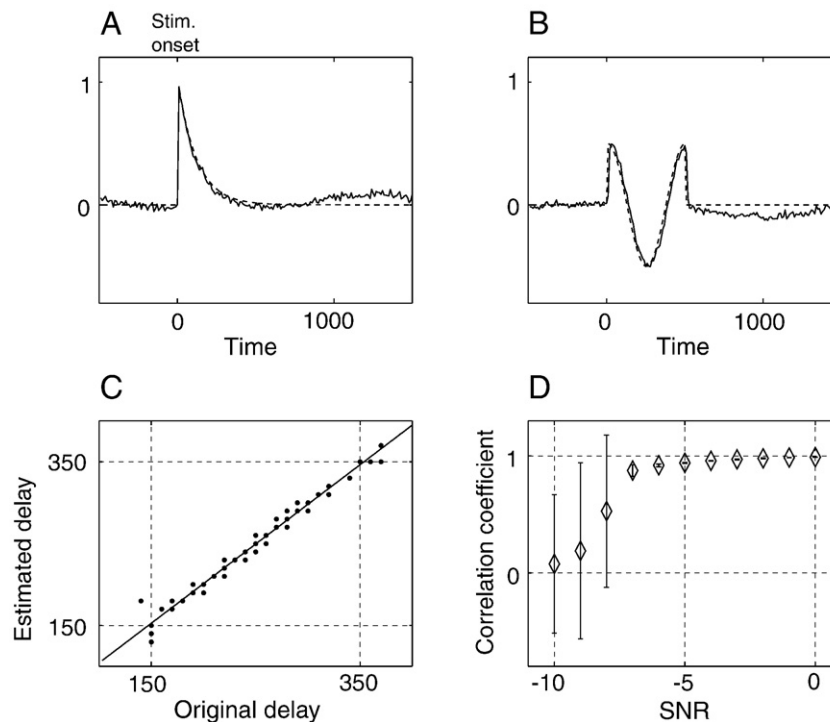


Fig. 3. Simulation with artificial data. (A–C) Examples of the extracted components and the estimated delays when the SNR is set to zero. (A) Extracted stimulus-locked component (solid line) and original one (dotted line). (B) Extracted stimulus-unlocked component (solid line) and original one (dotted line). The horizontal axis represents relative time to the defined onsets of the stimulus-unlocked component. (C) Scatter plot of the estimated and original delays. (D) Correlation coefficients between the estimated and original delays for each SNR. The diamonds and error bars respectively represent the means and SDs of the correlation coefficients.

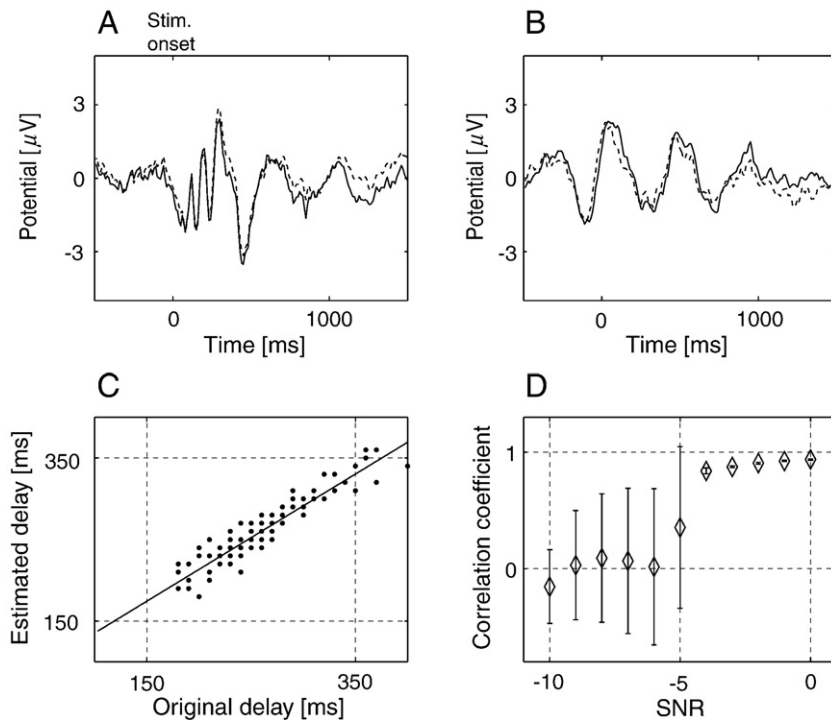


Fig. 4. Simulation with EEG data. (A–C) Examples of the extracted components and the estimated delays when the SNR is set to zero. (A) Extracted stimulus-locked component (solid line) and original one (dotted line). (B) Extracted stimulus-unlocked component (solid line) and original one (dotted line). The horizontal axis represents relative time to the defined onsets of the stimulus-unlocked component. (C) Scatter plot of the estimated and original delays. (D) Correlation coefficients between the estimated and original delays for each SNR. The diamonds and error bars respectively represent the means and SDs of the correlation coefficients.

viewing task. In the Go/NoGo task, the subjects undertook four experimental blocks, each consisting of 50 trials. The subjects were instructed to push a button immediately after a “Go” signal (green LED) or not to push it after a “NoGo” signal (red LED). The green or red LED was illuminated in random order with almost equal probability. In two blocks, the subjects had to respond with their right index finger, and in the other two blocks with their left index finger. In an off-line analysis, the data from the blocks of right and left fingers were mixed. In the passive viewing task, the subjects undertook two experimental blocks, each consisting of 50 trials. The subjects were instructed passively to view the same stimulus as in the Go/NoGo task. In both tasks, each trial began with a warning signal (a beep), followed, after a variable delay of 1.8–2.2 s, by the imperative signals (duration: 500 ms). Inter-trial intervals were randomized from 3.5 to 7.5 s.

During the tasks, surface EEG was recorded from 19-ch tin electrodes, mounted in a cap (Electro-Cap International, Inc., Eaton, Ohio, USA) according to the International 10–20 system, referred to a tin electrode placed on AFz. The EEG was amplified on a Nihon Kohden EEG-1100 with a time constant of 0.3 s. Because we expected that large EEG activity related to the task execution would not appear around the earlobes, we placed Ag/AgCl electrodes on both earlobes and recorded their potentials separately. Their averaged potentials were subtracted from the EEG data off-line. For monitoring eye movements, an electrooculogram (EOG) was recorded with a pair of Ag/AgCl electrodes placed above and below the left eye. The sampling rate of the EEG and EOG was 1000 Hz.

Data analysis

In an off-line analysis, we resampled the EEG data at a rate of 100 Hz. Because our previous method has the technical limitation that slow waves (~ 1 Hz) in the background EEG activity are amplified by the decomposition (Takeda et al., 2008), the EEG data were filtered with a bandpass of 2–40 Hz by using two kinds of finite impulse response (FIR) filters: a high-pass of 2 Hz (300-point, -26 dB at 1 Hz) and a low-pass of 40 Hz (15-point, -45 dB at 50 Hz). Then, the filtered EEG data were segmented into 2 s epochs from -500 to 1500 ms after stimulus onsets.

Reaction times of Go trials were defined as the intervals between the stimulus onset and the button push signal onset. We excluded Go trials with the RT either shorter than 100 ms or longer than 400 ms, and excluded NoGo trials with responses. An artifact criterion of $\pm 50 \mu\text{V}$ was used for the EEG and EOG to reject trials with excess ocular artifacts or measurement noise. The numbers of trials obtained per subject were 77 ± 12 for Go trials, 87 ± 13 for NoGo trials, and 78 ± 25 for the passive viewing task.

Application to EEG during Go trials

Because the EEG during Go trials consists of the stimulus- and response-locked components, i.e., the stimulus-locked and -unlocked components, it is expected that our method can estimate the RTs, i.e., the delays of the stimulus-unlocked component. To test this, we applied the proposed method to the individual subject's EEG data at Cz during Go trials for 10 times, and obtained 10 sets of estimated RTs. In estimating the RTs, we set the range of the RTs at the width of

300 ms. The accuracy of the estimated RTs was quantified by the correlation coefficient between the estimated and real RTs.

Check for existence of stimulus-unlocked component in EEG during NoGo trials

Although the proposed method assumes that EEG activity consists of the stimulus-locked and -unlocked components, the validity of this assumption, especially the existence of the stimulus-unlocked component, is not always guaranteed at least for the EEG during NoGo trials of the Go/NoGo task. As an alternative assumption, we might also consider that the EEG during NoGo trials includes only the stimulus-locked component. Therefore, in order to check whether the EEG included the stimulus-unlocked component or not, we examined the time course of the EEG variance across trials.

Suppose that the background noise is a stationary process, from the assumption of Eq. (1), the EEG variance across trials $Var[y(t)]$ is approximately expressed by:

$$Var[y(t)] \approx \frac{1}{N} \sum_{n=1}^N \left[r(t - \tau_n) - \frac{1}{N} \sum_{n=1}^N r(t - \tau_n) \right]^2 + Var[v], \quad (5)$$

where $Var[v]$ represents the variance of noise across trials. From Eq. (5), if the stimulus-unlocked component does not exist, the EEG variance is expressed by:

$$Var[y(t)] \approx Var[v]. \quad (6)$$

Eqs. (5) and (6) indicate that the time courses of the EEG variance are qualitatively different depending on whether the stimulus-unlocked component exists or not. If the stimulus-unlocked component exists, the variance should increase and decrease after stimulus onset because of the trial-to-trial variability in its delays. In contrast, if the stimulus-unlocked component does not exist, the variance should be constant. Therefore, we checked the existence of the stimulus-unlocked components by examining the time course of the EEG variance across trials (Fig. 5).

Application to EEG during NoGo trials

Because the variance of the EEG during NoGo trials at C3, C4, Fz and Cz showed a transient increase (Fig. 5), we applied the proposed method to these EEG data. We obtained the stimulus-

locked components, the stimulus-unlocked components and the delays for each subject and each channel. In estimating the delays, we set their range at the width of 400 ms, because the EEG variance was significantly greater than the pre-stimulus level for about 400 ms after the stimulus onset ($p < 0.05$, Wilcoxon signed-rank test).

To examine the robustness of the estimated delays, we repeated the estimation of the delays 10 times for the same EEG data, and obtained 10 sets of delays. The robustness was checked in the following way. First, we calculated the correlation coefficient between each set and the average of the other sets, and obtained the 10 correlation coefficients. Then, we conducted a two-tailed Wilcoxon signed-rank test to assess the null hypothesis that the correlation coefficients did not differ from zero. If the null hypothesis was not rejected at the alpha level of 0.05, we regarded the SNR of the EEG not to be high enough to estimate the delays robustly and excluded the EEG data from the following analyses. If the null hypothesis was rejected, we regarded the estimation results to be robust and, in the following analyses, used the set of delays whose correlation coefficient was the highest. As a result, we obtained the delays of 6 sets for C3, 6 sets for C4, 7 sets for Fz, and 6 sets for Cz, from the 9 subjects' EEG data during NoGo trials.

We adjusted the average of the delays so that the estimated delays represented latencies of the same peaks in the extracted stimulus-unlocked components across subjects. First, we set a subject's stimulus-unlocked components as references, and shifted the other subjects' delays and the stimulus-unlocked components so that their values of the cross-correlations with the references became maximum at the lag of zero. Then, we shifted all the subjects' delays so that the delays represented latencies of the maximum peaks in the average stimulus-unlocked components of all the subjects.

After the estimation, to examine the validity of the estimated delays, we formed time-trial images (Jung et al., 2001) of the EEG during NoGo trials sorted by the estimated delays (Fig. 6). In these images, all the subjects' EEG epochs were smoothed vertically with a 15-trial moving average, and the potential fluctuations were shown as color-coded horizontal lines. If the estimated delays are valid, both the stimulus- and estimated delay-locked fluctuations should appear, whereas, if the estimated delays are wrong, only the stimulus-locked fluctuations should appear, as shown in the left panel in Fig. 6. Therefore, we examined whether the estimated

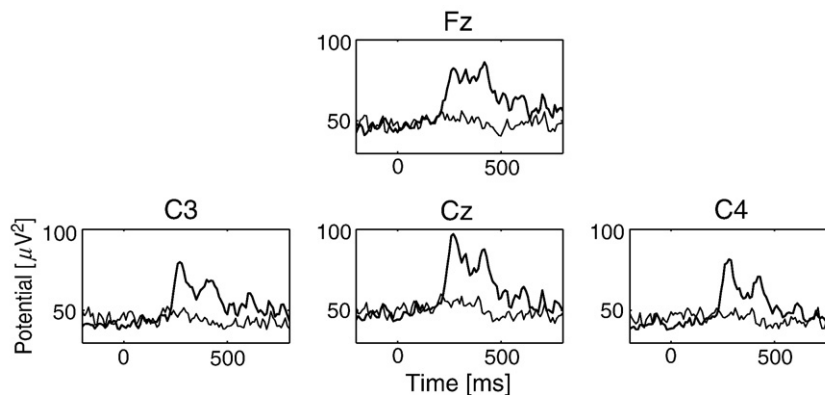


Fig. 5. Time course of the EEG variance across trials at C3, C4, Fz and Cz obtained from all the subjects' EEG. Thick lines represent the EEG variance during NoGo trials; thin lines represent the EEG variance during the passive viewing task.

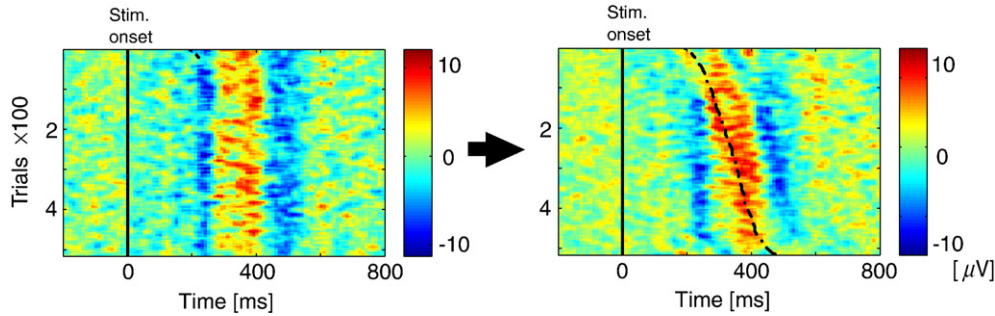


Fig. 6. Time-trial images of all the subjects' EEG at Cz during NoGo trials. In the left image, the EEG epochs are randomly sorted. In the right image, the EEG epochs are sorted by the estimated delays. The solid lines represent the stimulus onsets, and the dotted line represents the estimated delays.

delay-locked fluctuations appeared or not in the time-trial images of the EEG sorted by the estimated delays.

The similarity of the extracted components across subjects was quantified by calculating the correlation coefficient between a subject's component and the other subjects' average component for each subject, corresponding to the cross-correlation between the two waveforms at a lag of zero. As for the stimulus-locked components, the similarity of the extracted component to the stimulus-triggered average EEG was also quantified by the correlation coefficient between them. A two-tailed Wilcoxon signed-rank test was conducted to assess the null hypothesis that the correlation coefficients obtained from individual subjects did not differ from zero. An alpha level of 0.05 was used for the statistical tests.

Results

Simulation tests

Fig. 3 shows the results of the simulation test with artificial data. Examples of the extracted components and estimated delays from the simulated data with a SNR of 0 are shown in Fig. 3, A–C. The extracted stimulus-locked components are highly correlated with the original one ($r=0.96$) (Fig. 3, A), as are the extracted stimulus-unlocked components ($r=0.93$) (Fig. 3, B). The estimated delays are significantly correlated with the original ones ($r=0.99$, $p<0.05$, slope=0.96) (Fig. 3, C). This indicates that the performance of the method is adequately accurate when the SNR is 0. The correlation coefficients between the original and estimated delays from the simulated data with a SNR of $-10, \dots, 0$ are shown in Fig. 3, D. For a $SNR \geq -7$ (SD of the noise ≤ 0.39), the correlation coefficients are high in all the repeated estimations (Fig. 3, D), indicating that the estimation is adequately accurate and robust when the SNR is high. In contrast, for a $SNR < 7$ (SD of the noise > 0.39), the correlation coefficients are low and variable across the repeated estimations (Fig. 3, D), indicating that the estimation is neither accurate nor robust when the SNR is low.

Fig. 4 shows the results of the simulation test with EEG data. Examples of the extracted components and estimated delays from the simulated data with a SNR of 0 are shown in Fig. 4, A–C. The extracted stimulus-locked components are highly correlated with the original one ($r=0.94$) (Fig. 4, A), as are the extracted stimulus-unlocked components ($r=0.89$) (Fig. 4, B). The estimated delays are significantly correlated with the original ones ($r=0.94$, $p<0.05$, slope=0.78) (Fig. 4, C). This indicates that the performance of the method is adequately accurate when the SNR is 0. The correlation coefficients between the original and estimated delays from the

simulated data with a SNR of $-10, \dots, 0$ are shown in Fig. 4, D. For a $SNR \geq -4$ (SD of the noise ≤ 1.3), the correlation coefficients are high in all the repeated estimations (Fig. 4, D), indicating that the estimation is adequately accurate and robust when the SNR is high. In contrast, for a $SNR < -4$ (SD of the noise > 1.3), the correlation coefficients are low and variable across the repeated estimations (Fig. 4, D), indicating that the estimation is neither accurate nor robust when the SNR is low.

Estimation of RTs in Go trials

Table 1 shows the correlation coefficients between the real and estimated RTs from the individual subjects' EEG at Cz during Go trials by the proposed method. For Subjects 4 and 5, the estimated RTs are highly correlated with the real RTs (Table 1). For the other subjects, however, the estimated RTs are not correlated with the real RTs (Table 1).

Testing assumption for EEG during NoGo trials

Fig. 5 shows the time courses of the EEG variance during NoGo trials of the Go/NoGo task obtained from all the subjects' EEG. The variance of the EEG at C3, C4, Fz and Cz during NoGo trials shows transient increases during 300–500 ms after the stimulus onset (Fig. 5). In contrast, the variance is almost constant for the EEG during the passive viewing task (Fig. 5). This suggests that the EEG at these channels during NoGo trials includes the stimulus-unlocked component, whereas the EEG during the passive viewing of the same stimulus does not. Therefore, we apply our method to the EEG at C3, C4, Fz and Cz during NoGo trials.

Decomposing EEG during NoGo trials

Then, we obtain the stimulus-locked components, stimulus-unlocked components and the delays for individual EEG channels

Table 1
Correlation coefficients (r) between the estimated and real RTs in Go trials

| | Subj. 1 | Subj. 2 | Subj. 3 | Subj. 4 | Subj. 5 |
|-----|-------------------|-------------------|------------------|-------------------|------------------|
| r | -0.39 ± 0.061 | 0.017 ± 0.092 | 0.042 ± 0.15 | 0.37 ± 0.16 | 0.69 ± 0.043 |
| | Subj. 6 | Subj. 7 | Subj. 8 | Subj. 9 | |
| r | -0.097 ± 0.11 | -0.22 ± 0.25 | 0.17 ± 0.23 | -0.018 ± 0.11 | |

Values are mean \pm SD for 10 estimations.

and individual subjects. The estimated delays from the stimulus onsets, representing the latencies of the positive peaks in the stimulus-unlocked components, are 403 ± 76 ms for C3, 360 ± 66 ms for C4, 292 ± 78 ms for Fz, and 336 ± 69 ms for Cz, and these are much longer than the RTs of Go trials (269 ± 50 ms).

Fig. 6 shows the time-trial images obtained from all the subjects' EEG at Cz. When the EEG epochs are randomly sorted, only the stimulus-locked fluctuations appear (Fig. 6, left). However, when the EEG epochs are sorted by the estimated delays, not only the stimulus-locked but also the estimated delay-locked fluctuations appear (Fig. 6, right), suggestive of the validity of the estimated delays.

Fig. 7, A, shows the extracted stimulus-locked components for each EEG channel. The extracted components exhibit negative peaks at around 240 ms (N200) and positive peaks at around 370 ms (P300) after the stimulus onset for all the 4 channels. The correlation coefficients between the extracted components of individual subjects and the averaged components of the other subjects are significantly larger than zero ($r = 0.54 \pm 0.26$, $p < 0.05$ for C3; $r = 0.42 \pm 0.31$, $p < 0.05$ for C4; $r = 0.66 \pm 0.15$, $p < 0.05$ for Fz; $r = 0.43 \pm 0.31$, $p < 0.05$ for Cz), indicating that the extracted components exhibit similar patterns across subjects. The correlation coefficients between the extracted components and the stimulus-triggered average EEG are significantly larger than zero ($r = 0.90 \pm 0.049$, $p < 0.05$ for C3; $r = 0.87 \pm 0.12$, $p < 0.05$ for C4; $r = 0.94 \pm 0.050$, $p < 0.05$ for Fz; $r = 0.89 \pm 0.10$, $p < 0.05$ for Cz), indicating that the extracted stimulus-locked components exhibit similar patterns to the stimulus-triggered average EEG.

Conventionally, EEG activity related to a response inhibition is examined by using the NoGo-Go subtracting waveforms of the

stimulus-triggered average EEG (for example, Bokura et al., 2001; Falkenstein et al., 1999; Kok, 1988; Yamanaka et al., 2002). However, the stimulus-triggered average EEG is more or less contaminated by the temporal overlapping of the stimulus-unlocked components (Takeda et al., 2008). From the above-mentioned similarity between the extracted stimulus-locked component and the stimulus-triggered average EEG, it is expected that the difference in the stimulus-triggered average EEG between Go and NoGo trials comes from that of the stimulus-locked components rather than the contamination effects. To confirm this expectation, we compare the NoGo-Go subtracting waveforms of the stimulus-triggered average EEG with those of the stimulus-locked components. The stimulus-locked components of Go trials are extracted from the EEG and real RTs of Go trials by our previous method (Takeda et al., 2008). The NoGo-Go subtracting waveforms of the stimulus-triggered average EEG appear to be almost the same as those of the stimulus-locked components (Fig. 7, B), and the squared correlation coefficients between them are high ($r^2 = 0.59$ for C3; $r^2 = 0.70$ for C4; $r^2 = 0.94$ for Fz; $r^2 = 0.83$ for Cz). Therefore, it is suggested that, at around Fz and Cz, the differences of the stimulus-triggered average EEG between Go and NoGo trials are mainly (about 83–94%) attributable to those of the stimulus-locked components.

Fig. 8 shows the extracted stimulus-unlocked components for each EEG channel. The extracted stimulus-unlocked components exhibit positive peaks, whose magnitudes are comparable with those in the extracted stimulus-locked components. The correlation coefficients between the extracted components of individual subjects and the averaged components of the other subjects are significantly larger than zero ($r = 0.67 \pm 0.097$, $p < 0.05$ for C3; $r = 0.67 \pm 0.24$, $p < 0.05$ for C4; $r = 0.56 \pm 0.27$, $p < 0.05$ for Fz; $r = 0.67 \pm 0.17$,

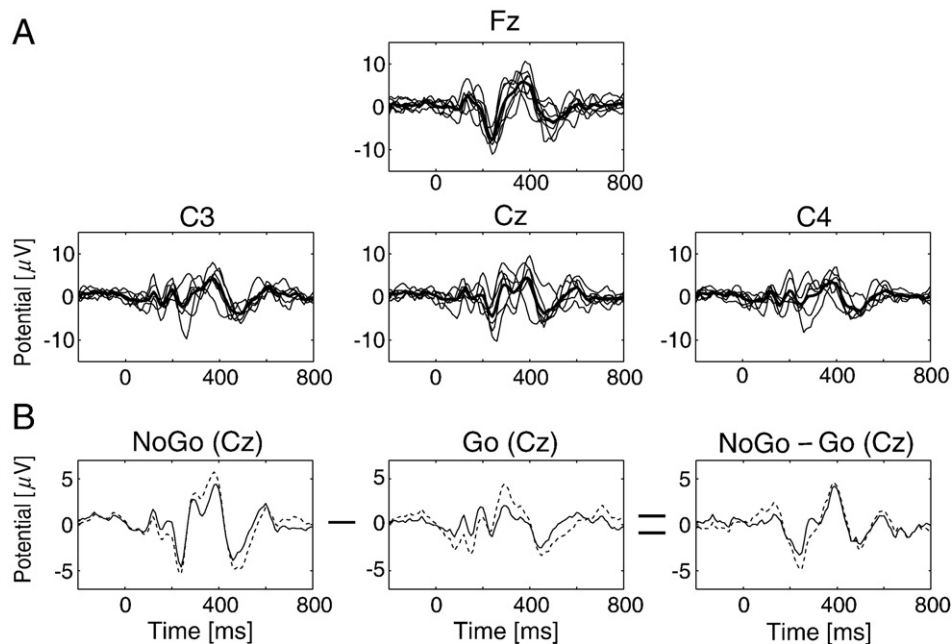


Fig. 7. Extracted stimulus-locked components at C3, C4, Fz and Cz. (A) Stimulus-locked components extracted from the EEG during NoGo trials. Thin lines represent the extracted stimulus-locked components of individual subjects, and thick lines represent the averaged components across subjects. (B) Differences of the extracted stimulus-locked components between Go and NoGo trials at Cz. The left panel shows the stimulus-locked component (solid line) and the stimulus-triggered average (dotted line) of NoGo trials. The middle panel shows the stimulus-locked component (solid line) and the stimulus-triggered average (dotted line) of Go trials. The right panel shows the NoGo-Go subtracting waveforms of the stimulus-locked component (solid line) and that of the stimulus-triggered average EEG (dotted line).

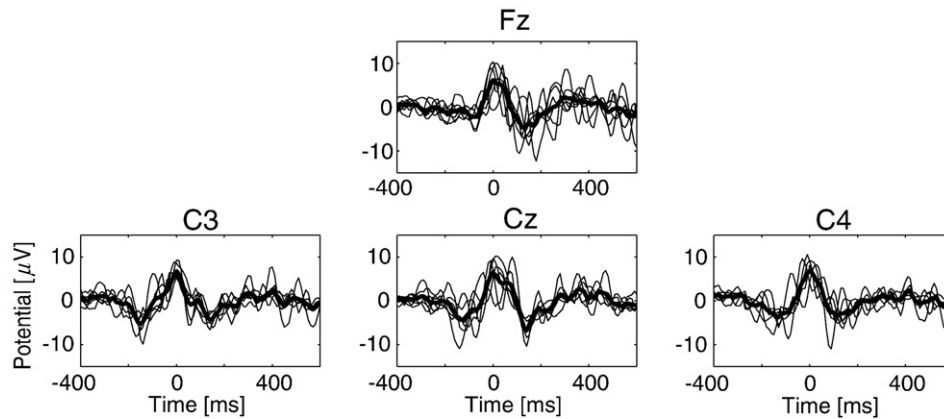


Fig. 8. Extracted stimulus-unlocked components from the EEG at C3, C4, Fz and Cz during NoGo trials. Thin lines represent the extracted stimulus-unlocked components of individual subjects, and thick lines represent the averaged components across subjects. The horizontal axes represent relative time to the time points of the maximum peaks in the average stimulus-unlocked components.

$p < 0.05$ for Cz), indicating that the extracted stimulus-unlocked components exhibit similar patterns across subjects.

Discussion

In this paper, we propose a novel method for obtaining the delays of the stimulus-unlocked components together with the stimulus-locked and -unlocked components only from single-channel EEG epochs. The performance of the algorithm is verified by two simulation tests with artificial and EEG data. Then, we apply this method to the EEG data during NoGo trials of the Go/NoGo task. As a result, the stimulus-unlocked components, together with the stimulus-locked components, are successfully extracted for the first time by this method.

Methodological considerations

The simulation tests show that our method can obtain the delays of the stimulus-unlocked component even from noisy data, the SNR of which is lower than zero but higher than -6 (for artificial data) or -3 (for EEG data) (Figs. 3 and 4, D). Here, the SNR lower than zero means that the level of the noise is larger than that of the signal. Generally speaking, when noise is larger than a signal, it is quite difficult, or impossible, to estimate the variable delays of the signal from single-trial data. Our method deals with the difficulty in a paradoxical way. To estimate the delays of “individual” trials, the method uses data epochs of “all” the trials in calculating the objective function. That is, we use all the trials for individual trials. This strategy is an essential point in the feasibility of our method for noisy data, such as EEG data.

The simulation tests also show that the estimation results become inaccurate when the SNR is lower than -7 (for artificial data) or -4 (for EEG data) (Figs. 3 and 4, D). It is of note that these results hold true only when the number of trials N is 100, and the accuracy of the estimation depends on the number of trials. When the number of trials is smaller, the waveforms of the components extracted by using true delays become less accurate. This indicates that the estimated delays obtained by searching for the delays which minimize the value of the objective function become less accurate. In contrast, when the number of trials is larger, the

waveforms of the components extracted by using true delays become more accurate. As a result, the true delays decrease the value of the objective function more adequately, and the estimated delays obtained by searching for the delays which minimize the value of the objective function become more accurate. In fact, in our simulation tests (not shown), as the number of trials increases, the correlation coefficients between the estimated and original delays become greater. Therefore, as long as we can solve the optimization problem, our method can overcome a higher noise level by increasing the number of trials.

In the optimization, we search for the set of the delays which minimizes the objective function. We adopt the random search for the optimization, because it achieves speedy convergence to a global minimum with a high probability. Generally speaking, a completely random search is a very slow algorithm when the number of trials N is large (see Fig. 2, A, thin solid line). This is because, as N increases, the size of the search space increases exponentially and the probability of finding an optimal set of delays decreases exponentially. We overcome this problem by searching for the delays sequentially. That is, we reduce the dimension of the search space from N to 1 by searching for the delays with respect to individual trials, and increase the probability to find a better set of delays. This is the reason why the convergence of the *restricted* random search we used is fast (Fig. 2, A, thick solid line), with a high probability of convergence to a global minimum (Fig. 2, B).

Because the random search is a stochastic algorithm, the estimated delays and the extracted components should vary more or less in each repeated estimation. The repeated simulation tests show that, when the SNR is high, the accuracy of the estimation is high and almost the same across the repetitions (Figs. 3 and 4, D), indicating that the estimation is robust when it is accurate. When the SNR is low, the accuracy of the estimation is low and variable across the repetitions (Figs. 3 and 4, D), indicating that the estimation is not robust when it is not accurate. From these results, it is suggested that the robustness can be an index of the accuracy of the estimation. Therefore, we repeatedly apply our method to the EEG during NoGo trials to check the robustness of the estimation results and present only robust results (see Methods section).

Hitherto, the waveforms and delays of the stimulus-unlocked EEG components have been obtained by peak-picking, Woody's

method and the method of Pham et al. (Biggins et al., 1997; Jaśkowski and Verleger, 1999, 2000; McGillem et al., 1985; Möcks et al., 1988; Pham et al., 1987; Puce et al., 1994a,b; Woody, 1967). The main difference between our method and these is the underlying assumption. These methods assume that only one component, the stimulus-unlocked component, appears after stimulus onsets, whereas our method assumes that two components, the stimulus-locked and -unlocked components, appear and these are temporally overlapping. The temporal overlapping of the two unknown components makes the problem quite difficult because the two components contaminate each other, and the appearance of the two components varies from trial to trial (see Fig. 1, B). For example, it is possible that a negative peak in the stimulus-locked component averages out a positive peak in the stimulus-unlocked component and both of the components appear not to have the peaks. Because methods which assume only one component do not consider such a contamination effect, they cannot be used when two components are temporally overlapping. In contrast, our method can be used, regardless of whether the number of the components is one or two and whether contamination occurs or not.

On the other hand, our method has a limitation. In calculating the objective function, the proposed method uses our previous method for decomposing EEG during reaction time tasks into stimulus- and response-locked components using known RTs (Takeda et al., 2008). This method has the technical limitation that slow waves (~1 Hz) in noise are amplified by the decomposition. Because of this limitation, the proposed method cannot easily deal with slow components, such as the contingent negative variation (Walter et al., 1964). To extract slow components by the proposed method, we need to increase the number of trials at the expense of the calculation time for the optimization.

Estimated RTs from EEG during Go trials

By applying our method to the EEG during Go trials, the RTs of Go trials are successfully estimated for Subjects 4 and 5, but are not for the other subjects (Table 1). The successes of the estimation support the feasibility of our method for real EEG data. On the other hand, the failures of the estimation are partially due to the low SNR of EEG during Go trials and to the fact that the stimulus-unlocked components are not necessarily time-locked to the motor responses. As for the latter, Verleger et al. (2005) examined the EEG during choice reaction time tasks by the stimulus- and response-triggered averaging procedures, and reported that the P3b is time-locked to neither stimulus nor motor response onsets. Considering that the Go/NoGo task is a choice reaction time task, it is possible that the EEG during Go trials also includes the components time-locked to neither stimulus nor motor response onsets and our method extracts such components instead of the response-locked components.

Extracted components from EEG during NoGo trials

This method assumes that the EEG activity consists of a stimulus-locked component and a stimulus-unlocked component. However, the existence of a stimulus-unlocked component is less evident than a stimulus-locked component, which appears with the use of the stimulus-triggered averaging procedure. Therefore, to check the validity of the assumption, we examine whether the EEG variance across trials shows a transient increase after the stimulus

onset. Although one might argue that the changes in the EEG variance are attributable to the variability of the waveform of the stimulus-locked component rather than the stimulus-unlocked component and its variable delays, from the relatively constant EEG variance during the passive viewing task, we believe that the variability of the waveform of the stimulus-locked component is not so large as to generate a drastic change in the variance of the EEG during NoGo trials (Fig. 5). Therefore, we apply the proposed method to the EEG during NoGo trials, and extract the stimulus-locked and -unlocked components.

The waveforms of the extracted stimulus-locked components are almost the same as those of the stimulus-triggered average EEG. This indicates that the stimulus-unlocked components are almost cancelled out by the stimulus-triggered averaging procedure. The extracted stimulus-locked components exhibit the N200 and P300 as well as the stimulus-triggered average EEG. This indicates that the N200 and P300, which are the classical peaks of the EEG during NoGo trials (Bokura et al., 2001; Falkenstein et al., 1999; Verleger, 1988; Verleger et al., 2006; Yamanaka et al., 2002), are stimulus-locked. We can visually confirm this fact by the stimulus-locked fluctuations at around 240 and 370 ms in the time-trial images (Fig. 6). At around Fz and Cz, the differences in the stimulus-locked components between Go and NoGo trials largely account for those in the stimulus-triggered average EEG (Fig. 7, B). This result suggests that, in the fronto-central region, the conventional differences in the EEG between Go and NoGo trials are mainly attributable to those in the stimulus-locked components rather than the contamination effects by the stimulus-unlocked components. Further, the different waveforms of the stimulus-locked component between Go and NoGo trials indicate that the stimulus-related brain processes are different between Go and NoGo trials.

As for the extracted stimulus-unlocked components, its magnitudes are comparable with those of the stimulus-locked components (Figs. 7 and 8). The presence of the extracted stimulus-unlocked components and the validity of the estimated delays are confirmed by the results that the time-trial images show the fluctuations time-locked to the estimated delays and that the waveforms of the extracted components are similar across subjects.

The average delays of the positive peaks in the stimulus-unlocked components are almost the same as the P300 latency in the stimulus-locked component (363 ± 26 ms), indicating that the positive peaks mainly overlap with the P300 in the stimulus-locked components (see Fig. 6, right). From this result, we consider that our method for the first time decomposes the conventional P300 of NoGo trials, which appears by the stimulus-triggered averaging procedure, into the stimulus-locked P300 and the stimulus-unlocked P300, corresponding to the positive peak in the stimulus-unlocked component.

Possible applicability

Our method extracts the stimulus-locked component, the stimulus-unlocked component and its delays of individual trials from the EEG data during NoGo trials. Then, what will be gained by applying our method to other EEG data (and possibly to other brain signals)?

Tallon-Baudry showed evidence for a role for induced gamma activity, whose phase is not time-locked to stimulus onset, in the construction of a coherent representation of objects and the rehearsal of the representation in memory (Tallon-Baudry and Bertrand, 1999). This suggests that some brain activity related to perception

and memory recall is not time-locked to stimulus onset. Also, the brain activity related to solving problems, or the “Aha!” experience (Jung-Beeman et al., 2004), is not time-locked to the presentation of problems. Until now, the time points of solving problems have been estimated from the onset of the subject's response claiming to have solved the problem (for example, Jung-Beeman et al., 2004). However, the relation between the onset of the solving of a problem and that of the subject's response is not clear. Considering the large variability of RTs even during “simple” reaction time tasks, it is possible that the intervals between the two onsets also have large variability. If so, we cannot extract pure brain activity related to problem solving from the response onset. By applying our method to EEG during these kinds of cognitive tasks, we can obtain more detailed information, the pure EEG waveform and its onsets, on the brain activity involved in such complex functions.

The advantages of our method are not only to extract the stimulus-unlocked component but also to extract the uncontaminated stimulus-locked component. Conventionally, the stimulus-triggered average EEG has been thought to reflect the stimulus-locked EEG component in the hope that the stimulus-unlocked component, even if it exists, would be cancelled out by the stimulus-triggered averaging procedure. However, whether this premise is well satisfied or not is unclear unless uncontaminated components are disclosed. This is because the effect of the contamination is determined by the waveform of the stimulus-unlocked component and its delays, which were unknown before the application of our method. In this study, we reveal that the contamination is small in the fronto-central region by comparing the NoGo-Go subtracting waveforms of the stimulus-triggered average EEG with those of the stimulus-locked components. By applying our method, we can obtain the uncontaminated stimulus-locked component and examine the level of contamination by the stimulus-unlocked component.

Conclusion

The proposed method successfully extracts a stimulus-unlocked component and its delays from the EEG during NoGo trials. In the brain, internal and subjective events related to cognitive functions seem to occur, not with precisely constant delays, but with various delays from trial to trial after stimulus onset. Since the proposed method can extract such brain activity, the method will provide a new tool to look into complex and implicit brain functions.

References

- Biggins, C.A., MacKay, S., Clark, W., Fein, G., 1997. Event-related potential evidence for frontal cortex effects of chronic cocaine dependence. *Biol. Psychiatry* 42, 472–485.
- Bokura, H., Yamaguchi, S., Kobayashi, S., 2001. Electrophysiological correlates for response inhibition in a Go/NoGo task. *Clin. Neurophysiol.* 112, 2224–2232.
- Braun, C.M.J., Villeneuve, L., Gruzeliier, J.H., 2002. Topographical analysis of stimulus-related and response-related electrical scalp activity and interhemispheric dynamics in normal humans. *Int. J. Psychophysiol.* 46, 109–122.
- David, O., Kilner, J.M., Friston, K.J., 2006. Mechanisms of evoked and induced responses in MEG/EEG. *NeuroImage* 31, 1580–1591.
- Endo, H., Kizuka, T., Masuda, T., Takeda, T., 1999. Automatic activation in the human primary motor cortex synchronized with movement preparation. *Cogn. Brain Res.* 3, 229–239.
- Falkenstein, M., Hoormann, J., Hohnsbein, J., 1999. ERP components in Go/NoGo tasks and their relation to inhibition. *Acta Psychol.* 101, 267–291.
- Goodin, D.S., Aminoff, M.J., Mantle, M.M., 1986. Subclasses of event-related potentials: response-locked and stimulus-locked components. *Ann. Neurol.* 20, 603–609.
- Haenschel, C., Baldeweg, T., Croft, R.J., Whittington, M., Gruzeliier, J., 2000. Gamma and beta frequency oscillations in response to novel auditory stimuli: a comparison of human electroencephalogram (EEG) data with in vitro models. *Proc. Natl. Acad. Sci. U. S. A.* 97, 7645–7650.
- Holland, J.H., 1975. *Adaptation in natural and artificial systems*. The Univ. Michigan Press.
- Jaśkowski, P., Verleger, R., 1999. Amplitudes and latencies of single-trial ERP's estimated by a maximum-likelihood method. *IEEE Trans. Biomed. Eng.* 46, 987–993.
- Jaśkowski, P., Verleger, R., 2000. An evaluation of methods for single-trial estimation of P3 latency. *Psychophysiology* 37, 153–162.
- Jung, T.-P., Makeig, S., Westerfield, M., Townsend, J., Courchesne, E., Sejnowski, T.J., 2001. Analysis and visualization of single-trial event-related potentials. *Hum. Brain Mapp.* 14, 166–185.
- Jung-Beeman, M., Bowden, E.M., Haberman, J., Frymiare, J.L., Arambel-Liu, S., Greenblatt, R., Reber, P.J., Kounios, J., 2004. Neural activity when people solve verbal problems with insight. *PLoS Biol.* 2, 500–510.
- Kirkpatrick, S., Gelatt Jr., C.D., Vecchi, M.P., 1983. Optimization by simulated annealing. *Science* 13, 671–680.
- Kirmizi-Alsan, E., Bayraktaroglu, Z., Gurvit, H., Keskin, Y.H., Emre, M., Demiralp, T., 2006. Comparative analysis of event-related potentials during Go/NoGo and CPT: decomposition of electrophysiological markers of response inhibition and sustained attention. *Brain Res.* 1104, 114–128.
- Kok, A., 1988. Overlap between P300 and movement-related-potentials: a response to Verleger. *Biol. Psychol.* 27, 51–58.
- Lamarre, Y., Busby, L., Spidalieri, G., 1983. Fast ballistic arm movements triggered by visual, auditory, and somesthetic stimuli in the monkey. I. Activity of precentral cortical neurons. *J. Neurophysiol.* 50, 1343–1358.
- McGillem, C.D., Aunon, J.I., Pomalaza, C.A., 1985. Improved waveform estimation procedures for event-related potentials. *IEEE Trans. Biomed. Eng.* 32, 371–379.
- Möcks, J., Köhler, W., Gasser, T., Pham, D.T., 1988. Novel approaches to the problem of latency jitter. *Psychophysiology* 25, 217–226.
- Nelson, R.J., 1987. Activity of monkey primary somatosensory cortical neurons changes prior to active movement. *Brain Res.* 406, 402–407.
- Nelson, R.J., Smith, B.N., Douglas, V.D., 1991. Relationships between sensory responsiveness and premovement activity of quickly adapting neurons in areas 3b and 1 of monkey primary somatosensory cortex. *Exp. Brain Res.* 84, 75–90.
- Perfiliev, S.N., 1998. Responses in the motor cortex time-locked to the sensory stimuli conditioning target-reaching in the cat. *Neurosci. Res.* 32, 273–279.
- Pham, D.T., Möcks, J., Köhler, W., Gasser, T., 1987. Variable latencies of noisy signals: estimation and testing in brain potential data. *Biometrika* 74, 525–533.
- Puce, A., Berkovic, S.F., Cadusch, P.J., Bladin, P.F., 1994a. P3 latency jitter assessed using 2 techniques. I. Simulated data and surface recordings in normal subjects. *Electroencephalogr. Clin. Neurophysiol.* 92, 352–364.
- Puce, A., Berkovic, S.F., Cadusch, P.J., Bladin, P.F., 1994b. P3 latency jitter assessed using 2 techniques. II. Surface and sphenoidal recordings in subjects with focal epilepsy. *Electroencephalogr. Clin. Neurophysiol.* 92, 555–567.
- Schürmann, M., Başar, E., 2001. Functional aspects of alpha oscillations in the EEG. *Int. J. Psychophysiol.* 39, 151–158.
- Takeda, Y., Yamanaka, K., Yamamoto, Y., 2008. Temporal decomposition of EEG during a simple reaction time task into stimulus- and response-locked components. *NeuroImage* 39, 742–754.
- Tallon-Baudry, C., Bertrand, O., 1999. Oscillatory gamma activity in humans and its role in object representation. *Trends Cogn. Sci.* 3, 151–162.
- Tallon-Baudry, C., Bertrand, O., Delpuech, C., Pernier, J., 1996. Stimulus specificity of phase-locked and non-phase-locked 40 Hz visual responses in human. *J. Neurosci.* 16, 4240–4249.

- Tanji, J., Kurata, K., 1982. Comparison of movement-related activity in two cortical motor areas of primates. *J. Neurophysiol.* 48, 633–653.
- Verleger, R., 1988. The true P3 is hard to see: some comments on Kok's (1986) paper on degraded stimuli. *Biol. Psychol.* 27, 45–50.
- Verleger, R., Jaśkowski, P., Wascher, E., 2005. Evidence for an integrative role of P3b in linking reaction to perception. *J. Psychophysiol.* 19, 165–181.
- Verleger, R., Paehge, T., Kolev, V., Yordanova, J., Jaśkowski, P., 2006. On the relation of movement-related potentials to the go/no-go effect on P3. *Biol. Psychol.* 73, 298–313.
- Walter, W.G., Cooper, R., Aldridge, V.J., McCallum, W.C., Winter, A.L., 1964. Contingent negative variation: an electric sign of sensori-motor association and expectancy in the human brain. *Nature* 203, 380–384.
- Woody, C.D., 1967. Characterization of an adaptive filter for the analysis of variable latency neuroelectric signals. *Med. Biol. Eng.* 5, 539–553.
- Yamanaka, K., Kimura, T., Miyazaki, M., Kawashima, N., Nozaki, D., Nakazawa, K., Yano, H., Yamamoto, Y., 2002. Human cortical activities during Go/NoGo tasks with opposite motor control paradigms. *Exp. Brain Res.* 142, 301–307.
- Zhigljavsky, A.A., 1991. *Theory of global random search*. Kluwer Academic Publishers.